BCMA-BBZ-OX40 CAR-T Therapy Using an Instant Manufacturing Platform or Traditional Production Process in Relapsed/Refractory Multiple Myeloma

Supplementary material

Principle investigator: Hui Liu

Department of Hematology, Beijing Hospital,

National Center of Gerontology, Institute of Geriatric Medicine,

Chinese Academy of Medical Sciences, Beijing, China

Table of Contents

1 Supplemental Figures

1.1 Figure legends.

Supplemental Figure 1. Antigen-independent OX40 enhanced CAR-T-cell function in vitro.

(A) Histogram of the expression of CAR and OX40 in T cells transduced with BCMA-BBZ-OX40 or BCMA-BBZ CAR constructs at different time points, data was collected from three donors; (B) In vitro cytotoxicity of T and BCMA CAR-T cells on H929 or U266 cells, bars indicate mean of three technical replicates with error bars indicating SD; (C) Representative quantification of PD-1 and LAG-3 on CAR-T cells after stimulation with U266 cells at E/T = 5/1 for four days; (D) Quantification of the expression of CD45RA and CD62L in CAR^+ T cells after stimulation with U266 cells at E/T = 5/1 for four days.

*p < 0.05, ***p < 0.001, ns > 0.05 by unpaired t test.

Supplemental Figure 2. Antigen-independent OX40 enhanced CAR-T-cell function in vivo.

(A) Schematics of the in vivo experimental workflow used, 2×10^6 CAR^+ T cells were injected into tumor-bearing mice; (B) representative bioluminescence imaging of the mouse model after CAR-T treatment; for all groups, n = 6; (C) Quantification showing the tumor burden as indicated by total radiance (p/ s/ cm2 /sr); (D) CAR^+ T-cell number in peripheral blood (PB) after CAR-T-cell injection; (E) survival curve of NPG mice with different treatments.

ns, not significant by unpaired Mann-Whitney test. For Kaplan-Meier curves, Log rank (Mantel-Cox) test was performed.

Supplemental Figure 3. Reduction of the manufacturing time improved CAR-T-cell function in vitro.

(A) Cell viability during seven days of recovery; (B) Proliferation of InstanCART and TraditionCART cells during seven days of recovery; (C) Histogram showing the phenotype of CAR^+ InstanCART and TraditionCART cells on day 7 after recovery; (D) Schema of restimulation of H929-LAE tumor cells in vitro; after four serial stimulations, BCMA-BBZ-OX40 CAR-T cells were cocultured with H929-LAE tumor cells for the in vitro killing assay; (E) histogram showing the viability and proliferation of CAR^+ InstanCART and

TraditionCART cells after four serial stimulations (indicated by black arrows) with H929-LAE tumor cells; (F) histogram showing the phenotype of CAR^+ InstanCART and TraditionCART cells after four serial stimulations with H929-LAE tumor cells; (G) the cytotoxicity of engineered InstanCART or TraditionCART cells against U266 tumor cells in vitro after four serial stimulations; (H) Experimental design of in vitro chronic stimulation model in which CAR-T cells were stimulated with 5×10^4 H929-LAE cells every three days. Red lines represent each round of restimulation with fresh H929-LAE target cells. On day 16 continuously stimulated CAR-T cells are analyzed by flow cytometry; (I) Total tumor cells remaining at the end of the stimulation; (J) CAR^+ T cells remaining at the end of the stimulation. CAR^+ T cells indicated T cells which expressed the CAR on the cell surface. CAR-T cells indicated the total T cell population with and without CAR expression. Bars indicate mean of three technical replicates with error bars indicating SD.

*$p < 0.05$, ***$p < 0.001$, ****$p < 0.0001$ by one-way ANOVA for multiple comparisons.

1.2 Supplemental Figure 1. Antigen-independent OX40 enhanced CAR-T-cell function in vitro.

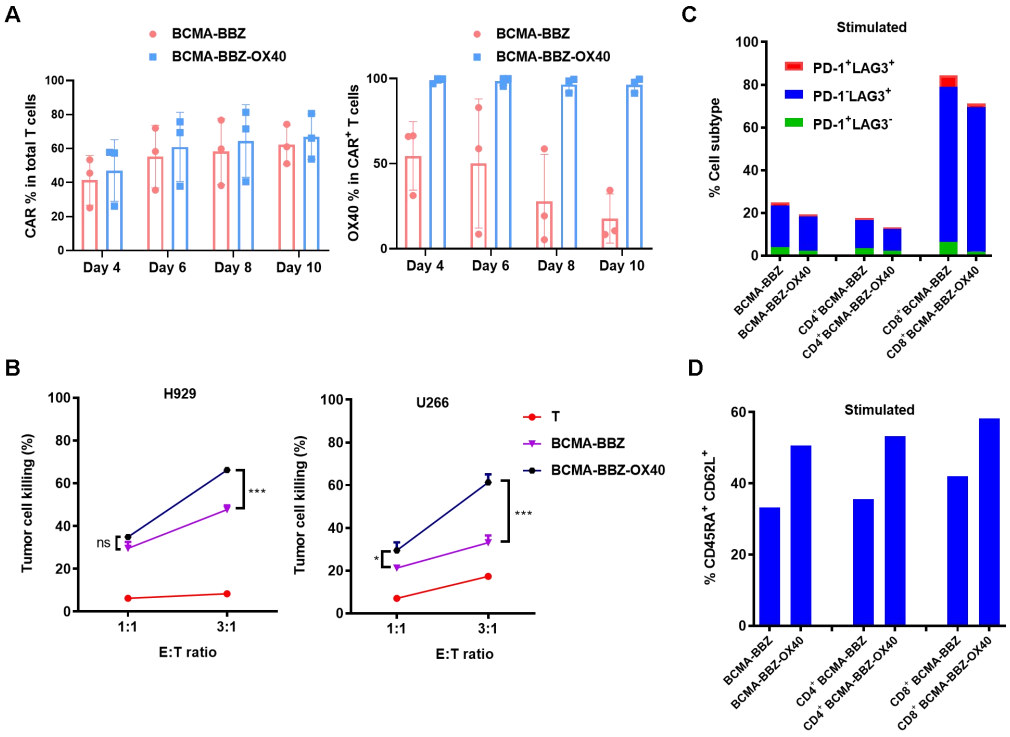

1.3 Supplemental Figure 2. Antigen-independent OX40 enhanced CAR-T-cell function in vivo.

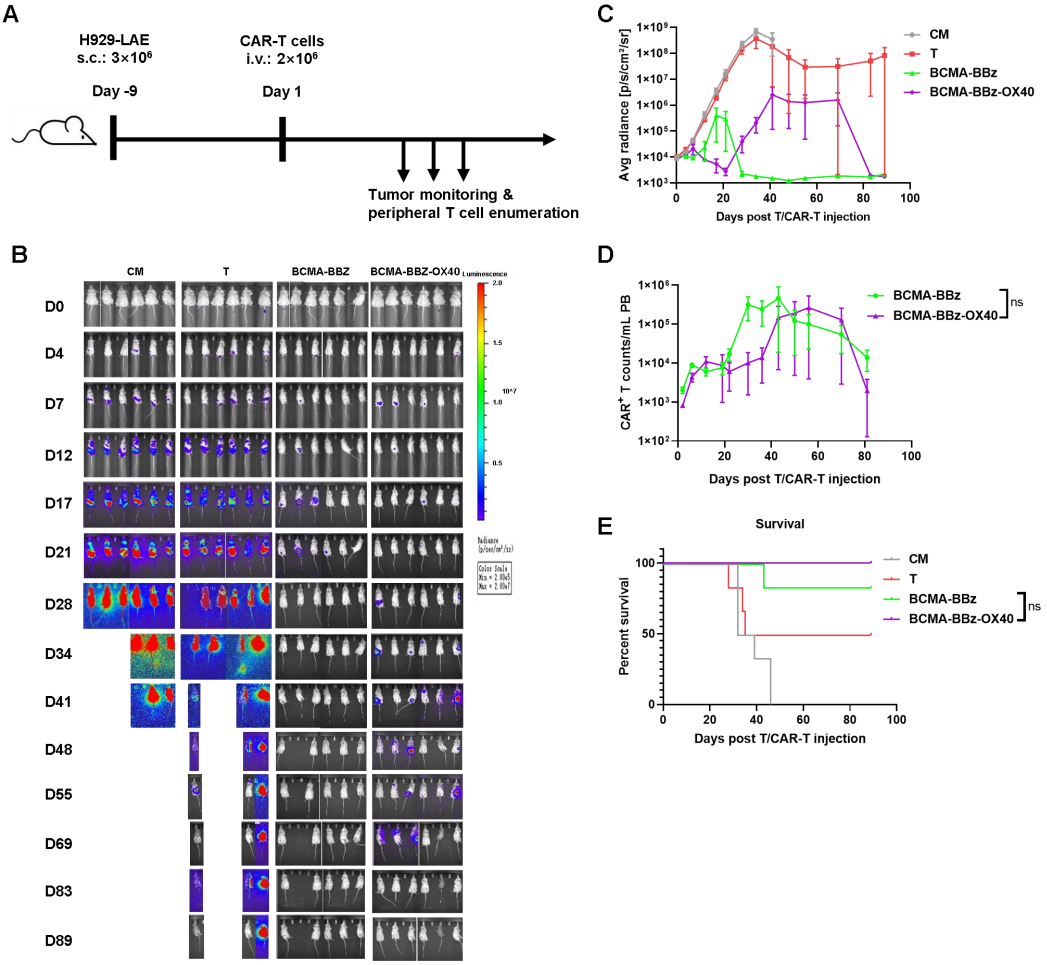

1.4 Supplemental Figure 3. Reduction of the manufacturing time improved CAR-T-cell function in vitro.

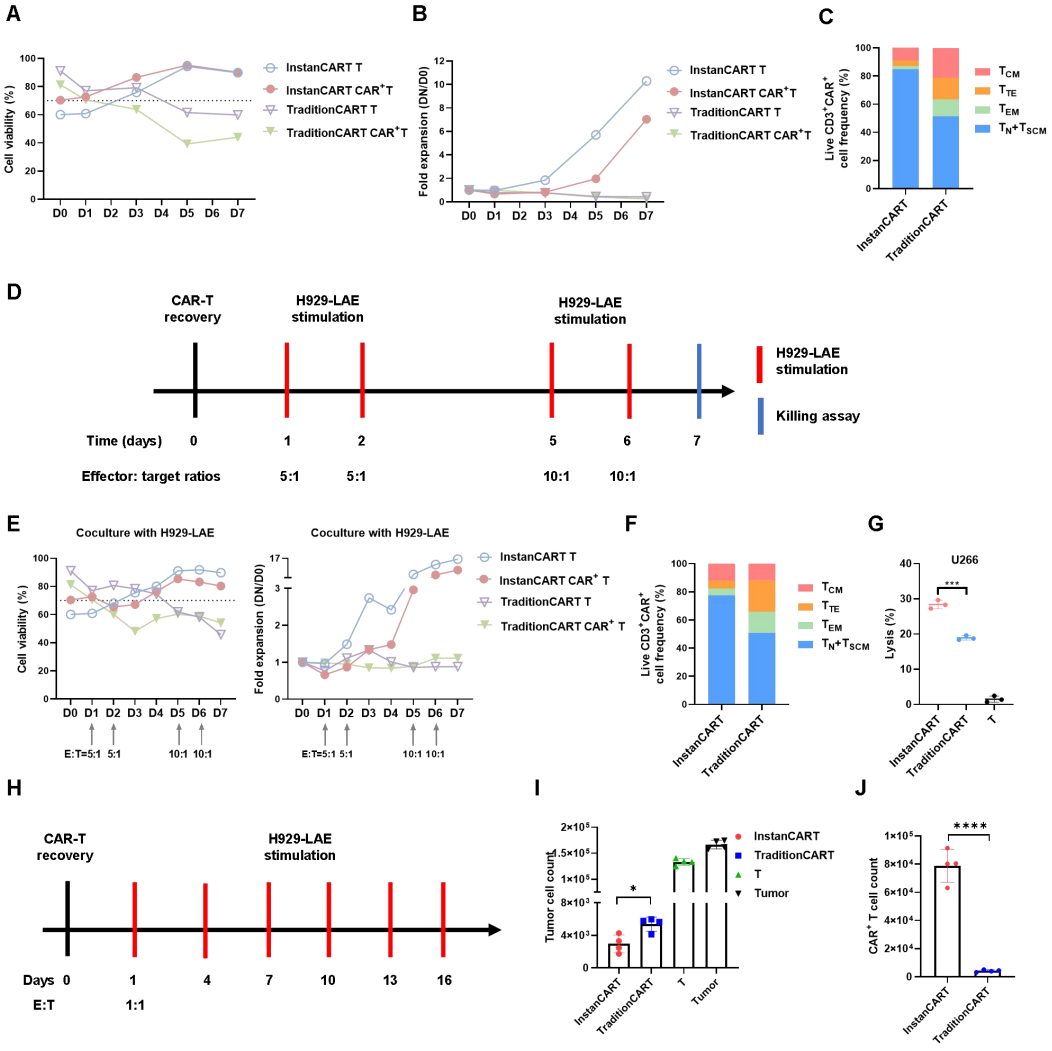

2 Supplemental Tables

2.1 Supplemental Table 1. Description of soft tissue plasmacytoma.

Patient ID	Sites of soft tissue plasmacytoma
BJ00	liver, spleen, multiple abdominal and subcutaneous nodules, cauda equina, the right parietal lobe region that was close to falx cerebri
BJ01	left supraclavicular fossa lymph node, masses on the left forehead, right lower back and left knee joint mass
BJ03	bone destruction of the left clavicle with soft tissue mass, multiple subcutaneous nodules in the chest and back
BJ04	pathological fracture of ribs with soft tissue mass, bilateral iliac soft tissue mass
BJ06	skull bone destruction with soft tissue mass
BJ08	bone destruction with soft tissue mass in the left iliac crest
BJ11	pancreas, liver, gallbladder, right kidney, right pleura and soft tissue mass at the right posterior tenth rib
BJ13	soft tissue lesions around some bones
BJ14	left lumbar mass, retroperitoneal para-aortic soft tissue, bilateral erector spinae, muscles around the pelvis, left sartorius, inguinal lymph nodes
BJ17	a right orbital mass, thickening and enhancement of the right frontotemporal and clivus dura mater, a soft tissue mass in front of the left ilium with unclear boundary with the iliacus muscle, and a local soft tissue mass in the cervical spine
BJ21	soft tissue masses at T9, left sixth and seventh ribs, left psoas major muscle, pancreatic neck, left pleura, chest wall and back
BJ22	left para-rib, thoracic paravertebral soft tissue masses, left pleural effusion in which clonal plasma cells were detected
BJ23	a soft tissue mass was found in the right proximal femur

2.2 Supplemental Table 2. Baseline characteristics of patients and clinical response after BCMA-BBZ-OX40 CAR-T cell therapy.

Patient number	Number of previous therapies	Immuno-globulin subtype	soft tissue plasmacytoma	Extramedullary disease	High risk cytogenetic profile	Triple-class refractory	Previous autologous stem-cell transplantation	ECOG PS	TraditionCART or InstanCART	Total CAR T or T cells infused	CRS	Neurological toxicity	Best response
BJ00	4	IgA-λ	1	1	1	1	1	4	TraditionCART	6.6×10^7 (CAR-T)	Grade 1	Grade 1	sCR
BJ01	6	IgA-κ	1	1	1	0	0	3	TraditionCART	6.5×10^7 (CAR-T)	Grade 1	None	VGPR
BJ03	3	IgG-λ	1	1	0	1	1	0	TraditionCART	18×10^7 (CAR-T)	Grade 1	None	PR
BJ04	4	IgA-λ	1	0	1	1	0	3	TraditionCART	8.4×10^7 (CAR-T)	Grade 1	None	CR
BJ05	3	λ	0	0	0	1	0	0	TraditionCART	8.3×10^7 (CAR-T)	Grade 1	None	sCR
BJ06	4	κ	1	0	1	1	0	4	TraditionCART	6.0×10^7 (CAR-T)	Grade 2	None	CR
BJ08	5	IgA-λ	1	0	0	0	0	0	TraditionCART	4.8×10^7 (CAR-T)	None	None	sCR
BJ09	3	IgA-λ	0	0	1	0	0	1	TraditionCART	6.8×10^7 (CAR-T)	Grade 1	None	VGPR
BJ10	2	λ	0	0	1	1	0	2	InstanCART	2.4×10^7 (T)	Grade 1	Grade 1	sCR
BJ11	4	IgG-λ	1	1	0	1	1	0	InstanCART	1.7×10^7 (T)	Grade 1	None	PR
BJ12	5	IgG-κ	0	0	1	0	1	0	InstanCART	2.3×10^7 (T)	Grade 1	None	VGPR
BJ13	7	IgD-λ	1	0	0	1	1	0	InstanCART	1.4×10^7 (T)	Grade 2	None	sCR
BJ14	3	IgG-κ	1	1	1	1	0	1	InstanCART	2.1×10^7 (T)	Grade 2	None	PR
BJ15	3	IgA-λ	0	0	0	0	0	1	InstanCART	1.8×10^7 (T)	Grade 1	None	sCR
BJ16	2	IgA-κ	0	0	0	0	0	1	TraditionCART	6.4×10^7 (CAR-T)	Grade 1	None	sCR
BJ17	3	IgA-λ	1	1	1	1	1	1	InstanCART	1.9×10^7 (T)	Grade 1	None	PR
BJ18	3	IgG-κ	0	0	1	0	0	2	TraditionCART	14×10^7 (CAR-T)	Grade 1	None	sCR
BJ19	2	IgA-λ	0	0	0	1	0	1	TraditionCART	16×10^7 (CAR-T)	Grade 1	None	sCR

BJ20	3	IgA-λ	0	0	0	1	0	1	TraditionCART	18×10^7 (CAR-T)	None	None	sCR
BJ21	4	IgG-κ	1	1	0	1	1	3	TraditionCART	20×10^7 (CAR-T)	Grade 1	None	PR
BJ22	2	IgA-λ	1	1	0	1	1	2	TraditionCART	7.9×10^7 (CAR-T)	Grade 1	None	sCR
BJ23	7	λ	1	0	1	1	1	3	TraditionCART	4.1×10^7 (CAR-T)	None	None	sCR